https://doi.org/10.5194/egusphere-2026-6335
Preprint. Discussion started: 6 November 2026
© Author(s) 2026. CC BY 4.0 License.

Sequential rainwater chemistry constrains in-cloud and below-cloud scavenging at a high-elevation site under contrasting transport regimes

Yucheng Chen[1,4], Baozhu Ge[1,*], Nuohang Liu[1,2], Lingkai Dong[1,2], Xiaole Pan[1], Xueling Cheng[1], Liquan Yao[3], Jinyuan Xin[1], Yele Sun[1], Feili Li[4,*], Lanzhong Liu[1], and Zifa Wang[1,2]

[1]State Key Laboratory of Atmospheric Environment and Extreme Meteorology, Institute of Atmospheric Physics, Chinese Academy of Sciences, Beijing, 100029, China
[2]University of Chinese Academy of Sciences, Beijing 100049, China
[3]Henan Institute of Science and Technology, Xinxiang, 453003, China
[4]College of Environment, Zhejiang University of Technology, Hangzhou 310032, China

Correspondence author: Baozhu Ge (gebz@mail.iap.ac.cn) and Feili Li (lifeli@zjut.edu.cn)

Abstract. High-elevation receptors in monsoon Asia intercept cloud-bearing regional air, yet the event-scale transition from below-cloud removal to a cloud-dominated precipitation signature remains poorly constrained. We collected 203 sequential rainwater fractions from 55 precipitation events in 2023 at the Atmospheric Boundary Layer Eco-Environment Shanghuang Observatory (ABLES; 1128 m a.s.l.) in southeastern China, where complex terrain and frequent cloud occurrence expose the site to contrasting continental and marine transport. Twelve events with at least six fractions were analysed using major-ion chemistry, two independent late-stage baseline estimates, backward trajectories, and reanalysis fields, with near-surface meteorological and turbulence observations available for R3–R6. Anthropogenic-type events began with the largest ionic loads and strongest early decreases, dominated by sulfate, nitrate, and ammonium. Marine-type events had lower but more variable concentrations, whereas calcium persisted relative to secondary inorganic ions in crustal-type events. Median estimated in-cloud contributions were 51.1 % for sulfate, 58.4 % for nitrate, and 49.2 % for ammonium, with event values exceeding 80 %. These fractions exceeded compiled urban medians but overlapped remote-environment ranges. Although not a direct cloud-water measurement, the 0.32 mg L^{-1} late-event sulfate baseline was one to two orders of magnitude below historical Chinese mountain cloud-water observations and reached the lower range of global mountain records, consistent with sulfur controls extending beyond surface air. By resolving source-dependent within-event transitions hidden by bulk sampling, this study establishes an event- and ion-specific observational benchmark for wet scavenging at an inland mountain receptor and clarifies how continental–marine transport conditions the precipitation signature.

1 Introduction

Wet deposition is one of the principal atmospheric sinks for soluble gases and aerosol particles and a major pathway by which reactive sulfur and nitrogen, sea salt, and mineral material are transferred to terrestrial and aquatic ecosystems. Its magnitude

https://doi.org/10.5194/egusphere-2026-6335
Preprint. Discussion started: 6 November 2026
© Author(s) 2026. CC BY 4.0 License.

and chemical composition influence atmospheric lifetimes, ecosystem nutrient supply, and acidification, while errors in wet removal propagate into assessments of regional transport and deposition exposure. Wet deposition combines in-cloud scavenging (ICS), in which trace constituents are incorporated during cloud formation and processing, and below-cloud scavenging (BCS), in which falling hydrometeors collect gases and particles below cloud base (Seinfeld and Pandis, 2016). The relative importance of the two pathways depends on aerosol abundance, particle size and hygroscopicity, gas solubility, vertical chemical structure, cloud microphysics, rainfall intensity, and drop-size distributions (Cheng et al., 2021; Wang et al., 2021; Jones et al., 2022). Observational separation of the pathways is therefore essential for understanding how cloud and precipitation processes regulate atmospheric composition.

Conventional event-integrated or daily precipitation samples measure total deposition but average over rapidly changing conditions. The first millimetres of rainfall can contain material accumulated below cloud before the event, whereas later fractions may increasingly reflect precipitation formed and processed aloft. Sequential sampling preserves this evolution. Studies in Beijing, Shanghai, Nanchang, Paris, and other locations commonly report high initial ion concentrations followed by a nonlinear decrease as rainfall proceeds (Ge et al., 2021; Xie et al., 2022; Zou et al., 2022; Audoux et al., 2023a, 2023b). Such records provide an empirical basis for representing the late-event concentration as a cloud-dominated precipitation baseline and the excess above it as additional below-cloud loading. The approach is valuable because direct, simultaneous sampling of cloud water, sub-cloud aerosols, gases, and precipitation is rarely available for a large set of natural rainfall events. The empirical partition is not a direct measurement of either process. Late-stage rainwater is not identical to cloud water: it has undergone descent, evaporation, collision, and possible exchange with the sub-cloud atmosphere. A concentration decline can also reflect dilution by increasing rainfall intensity, changes in drop-size distribution, transitions between rain cells, or changes in the air mass supplying the event. Conversely, sub-cloud replenishment and intermittent sources can generate concentration rebounds (Bayramoğlu Karşı et al., 2018; Berberler et al., 2022; Audoux et al., 2023b). An estimate based on the late-stage baseline must therefore report fit performance, test sensitivity to an alternative baseline, and distinguish the relative partition of event deposition from cloud-water concentration or absolute scavenging strength. Without these safeguards, a large inferred ICS fraction may be overinterpreted as evidence of chemically concentrated cloud water.

High-elevation observatories offer a particularly informative setting in which to examine this problem. Mountain sites can alternate between air influenced by the planetary boundary layer, residual layers, free-tropospheric flow, and cloud-bearing regional transport. Orographic ascent can lift moist marine or polluted air toward cloud level, while precipitation falling to the station can encounter a chemically distinct layer below cloud. Elevation also shortens the atmospheric column available for additional below-cloud collection relative to many lowland sites. Consequently, the same relative ICS fraction may have a different physical meaning at an elevated receptor than at an urban surface site. Observations from the European Alps, southern Africa, the Himalayas, and Asian karst mountains show that topography and air-mass pathway strongly condition precipitation chemistry (Zeng et al., 2022; Balestrini et al., 2024; Kok et al., 2024; Paudel Adhikari et al., 2024), but most mountain datasets remain event-integrated, daily, or seasonal. This evidence leaves two connected gaps. First, it is unclear whether large estimated ICS contributions at elevated or remote sites primarily indicate enhanced processing within clouds, limited additional

https://doi.org/10.5194/egusphere-2026-6335
Preprint. Discussion started: 6 November 2026
© Author(s) 2026. CC BY 4.0 License.

material below cloud, or a combination of both. Addressing this ambiguity requires simultaneous consideration of relative partition and absolute ion concentration. Second, the way contrasting continental, coastal, and marine transport regimes alter the transition from early to late rainfall is not well established. A marine pathway may reduce anthropogenic loading, but coastal passage and vertically different trajectories can produce mixed chemical signatures. Likewise, a crustal signature does not establish where mineral particles entered the precipitating system. Event-resolved observations are needed to determine which contrasts are reproducible and which remain specific to individual storms.

The Atmospheric Boundary Layer Eco-Environment Shanghuang Observatory (ABLES) is well suited to this test. It is located at 1128 m a.s.l. in the complex terrain of southeastern China, a region affected by the East Asian monsoon circulation, cloud and fog, continental outflow, and marine transport. Its limited local industrial influence but varied regional inputs make it suitable for examining pollutant wet removal under low ionic loading. Event-resolved measurements can separate initial loading, early removal, and late-event concentrations that event totals may conceal. Because source strength, elevation, sub-cloud path, and precipitation differ among urban, mountain, coastal, and remote sites, comparisons should retain absolute concentrations, baseline definitions, and fit diagnostics. We therefore use other environments as context and assess whether the high fraction of ICS at ABLES reflects cloud-level loading or limited uptake below cloud. In this study, 203 sequential rainwater samples collected during 55 events in 2023 are used to determine how source composition and transport background condition event-scale wet-scavenging signatures at ABLES. Twelve events containing at least six fractions are examined in detail. The objectives are to 1) establish the overall chemical setting and identify predominant anthropogenic-, marine-, and crustal-type event signatures; 2) quantify the within-event evolution of major ions and estimate relative ICS and BCS contributions using an exponential baseline and a final-three-fraction alternative; 3) compare the high-elevation estimates with urban and remote observations while separating relative fractions from absolute loading; and 4) use multi-height trajectories, reanalysis fields, and near-surface meteorological and turbulence observations for the overlapping events to define the transport and rainfall context without inferring an unobserved vertical chemical pathway. The central contribution is an event- and ion-resolved observational benchmark for interpreting cloud-dominated precipitation signatures at an inland mountain receptor.

2 Data and methods

2.1 Site and sequential rainwater sampling

Rainwater samples were collected at the Atmospheric Boundary Layer Eco-Environment Shanghuang Observatory (ABLES; 28.58° N, 119.51° E; 1128 m a.s.l.), located on the summit of Damaojian Mountain in Shanghuang Village, Jinhua, Zhejiang Province, southeastern China. The observatory is situated in a subtropical monsoon region characterized by complex mountainous terrain, prolonged precipitation during the Meiyu season, and frequent cloud and fog in early summer and autumn. No major industrial emission sources are located in the immediate vicinity of the site. Owing to its elevated position near the upper part of the regional atmospheric boundary layer, ABLES provides a suitable setting for investigating precipitation

https://doi.org/10.5194/egusphere-2026-6335
Preprint. Discussion started: 6 November 2026
© Author(s) 2026. CC BY 4.0 License.

chemistry under regional background conditions and the effects of cloud processes and regional atmospheric transport on wet deposition (Wang et al., 2026).

Sequential rainwater sampling was conducted during the 2023 observation period using an automatic wet–dry deposition sampler (APS-3A, Changsha Xianglan Scientific Instruments Co., Ltd., China). Following Ge et al. (2021), consecutive rainwater fractions were collected at rainfall-depth intervals of 1 mm, except for the final fraction. After the preceding bottles had each collected the equivalent of 1 mm of rainfall, the final bottle collected all remaining precipitation until the end of the event. The final fraction therefore did not necessarily represent 1 mm of rainfall. Successive precipitation separated by a rain-free interval of at least 2 h was treated as a new rainfall event. This sampling design resolved changes in rainwater chemistry from the beginning to the later stages of individual events. During the 2023 observation period, a total of 203 sequential rainwater samples were collected from 55 precipitation events.

2.2 Chemical analysis and quality control

Rainwater samples were refrigerated at 0–4 °C and analysed within one month. Four anions (F^-, Cl^-, NO_3^-, and SO_4^{2-}) and five cations (NH_4^+, Na^+, K^+, Mg^{2+}, and Ca^{2+}) were quantified using ion chromatography (Dionex 600, USA). Analytical reproducibility was evaluated using replicate measurements, with relative standard deviations below 5 % for all measured ions. Certified reference materials produced by the National Research Center for Certified Reference Materials, China, were used for routine quality assurance. Ultrapure-water blanks were analysed following the same procedure, and reported concentrations were corrected for blank contributions. Ionic consistency was additionally assessed using the event-level relationship between measured cation and anion equivalents. This regression is a dataset-level diagnostic rather than proof of complete electroneutrality because relevant ions were not measured. Electrical conductivity was not measured and was not used as a quality-control criterion. Further analytical and QA/QC details are provided by Ge et al. (2016) and Xu et al. (2017).

2.3 Data processing and event classification

Event-level volume-weighted mean concentrations from all 55 precipitation events were included in the Pearson correlation analysis and principal component analysis (PCA). Detailed intra-event analysis was restricted to events containing at least six sequential fractions. Twelve events met this criterion and were designated R1–R12. The selection criterion was independent of chemical composition and of the event types assigned subsequently. Total ion concentration was defined as the sum of the nine measured inorganic ions; unmeasured bicarbonate, carbonate, organic acids, and hydrogen ion were not included.

The volume-weighted mean (VWM) concentration of each ion was calculated for individual rainfall events and for the entire observation period as follows:

$$C_{\mathrm{VWM},j} = \frac{\sum_{i=1}^{n} c_{i,j} P_i}{\sum_{i=1}^{n} P_i} \quad (1)$$

https://doi.org/10.5194/egusphere-2026-6335
Preprint. Discussion started: 6 November 2026
© Author(s) 2026. CC BY 4.0 License.

where $C_{VWM,j}$ is the volume-weighted mean concentration of ion j, $C_{i,j}$ is its concentration in sequential fraction i, P_i is the corresponding rainfall amount, and n is the total number of fractions included in the calculation. Depending on the aggregation, the equation was applied either to an individual rainfall event or to all samples collected during the observation period. Event-level sums of the measured cations (ΣC) and anions (ΣA) were calculated on an equivalent-concentration basis, and ordinary least-squares linear regression was performed between ΣA and ΣC.

The non-sea-salt fraction of each ion was estimated using Na^+ as the sea-salt reference species:

$$C_{\mathrm{nss}-X} = C_X - C_{\mathrm{Na^+}} \left(\frac{X}{\mathrm{Na^+}}\right)_{\mathrm{seawater}} \quad (2)$$

where C_X and C_{Na^+} are the event-level volume-weighted mean concentrations of ion X and Na^+, respectively, and $(X/Na^+)_{seawater}$ is the corresponding mass ratio in seawater (Keene et al., 1986; Zhang et al., 2007). Non-sea-salt sulfate (nss-SO_4^{2-}) and non-sea-salt calcium (nss-Ca^{2+}) were used in the subsequent analysis of the source-related chemical characteristics of the rainfall events.

Statistical analyses were performed using IBM SPSS Statistics 23. Pearson correlation analysis was applied to the event-level concentrations of the nine measured ions from all 55 rainfall events, with significance evaluated using two-tailed tests. Correlations with $p < 0.01$ were considered significant. The coefficients described pairwise covariation and supported, rather than independently determined, the source-related interpretation of the PCA results.

PCA was conducted on the correlation matrix of the same 55-event dataset to identify the major patterns of covariation among the nine ions. Dataset suitability was evaluated using the Kaiser–Meyer–Olkin statistic and Bartlett's test of sphericity. Varimax orthogonal rotation was applied to facilitate interpretation. The first three rotated components that exhibited coherent chemical patterns were retained for source-related interpretation, and their scores for the 12 events containing at least six sequential fractions were extracted for subsequent event classification.

2.4 Estimation of in-cloud and below-cloud scavenging contributions and uncertainty

Sequential rainwater samples were used to estimate the relative contributions of in-cloud and below-cloud scavenging to ionic wet deposition. The framework assumes that the additional contribution acquired below cloud generally decreases as rainfall removes soluble material from the sub-cloud atmosphere. Later fractions are therefore used to estimate a cloud-dominated precipitation baseline (Aikawa and Hiraki, 2009; Ge et al., 2021). This baseline is derived from the sequential observations and is not a direct measurement of cloud-water composition.

Following Ge et al. (2021), the across-event median sequential concentration profile of each ion was fitted against cumulative rainfall depth using an exponential model:

$$y = C + Ae^{-kx} \quad (3)$$

where y is the median ion concentration at cumulative rainfall depth x, A is the initial concentration excess above the fitted baseline, k is the decay coefficient, and C is the fitted asymptotic concentration. This baseline is denoted C_{cloud} in the partition equations below. A positive asymptote from an acceptable median-profile fit was used as the common baseline for that ion

https://doi.org/10.5194/egusphere-2026-6335
Preprint. Discussion started: 6 November 2026
© Author(s) 2026. CC BY 4.0 License.

across all selected events. For an ion without an acceptable fit, the arithmetic mean concentration of the final three valid fractions of each rainfall event was used as its event-specific baseline.

The below-cloud wet-deposition loading of each ion was calculated as:

$$\mathrm{Wetdep}_{\mathrm{below-cloud}} = \sum_{i=1}^{n} \max(C_i - C_{cloud}, 0) P_i \quad (4)$$

where C_i is the concentration of a given ion in rainfall fraction i, P_i is the rainfall amount represented by fraction i, and n is the total number of sequential fractions collected during the event. When C_i was lower than C_{cloud}, the corresponding concentration difference was set to zero. When C_i is expressed in mg L^{-1} and P_i in mm, the resulting wet-deposition loading is expressed in mg m^{-2}.

The percentage contribution of below-cloud scavenging was calculated as:

$$\mathrm{Contribution}_{\mathrm{below-cloud}} = \frac{\mathrm{Wetdep}_{below-cloud}}{\sum_{i=1}^{n} C_i P_i} \times 100\ \% \quad (5)$$

After the below-cloud contribution was determined, the in-cloud scavenging contribution was calculated as:

$$\mathrm{Contribution}_{\mathrm{in-cloud}} = 100\ \% - \mathrm{Contribution}_{below-cloud} \quad (6)$$

Fit performance for the median concentration profiles was evaluated using the coefficient of determination (R^2), root-mean-square error (RMSE), and mean signed residual. The residual was defined as the observed median concentration minus the corresponding fitted concentration:

$$RMSE = \sqrt{\frac{1}{m} \sum_{j=1}^{m} (C_{obs,j} - C_{fit,j})^2} \quad (7)$$

$$\bar{e} = \frac{1}{m} \sum_{j=1}^{m} (C_{obs,j} - C_{fit,j}) \quad (8)$$

where m is the number of median-profile observations included in the fit, and $C_{obs,j}$ and $C_{fit,j}$ are the observed and fitted concentrations. R^2 describes the variation represented by the fitted curve, RMSE describes the magnitude of the concentration deviations, and the sign of the mean residual indicates overall under- or overprediction. These diagnostics assess fit performance, not parameter uncertainty. The results are presented in Table 2; event-specific final-three-fraction means are provided in Table S4.

2.5 Backward-trajectory and reanalysis analyses

To characterize the transport background at the onset of the selected rainfall events, 72 h backward trajectories arriving at ABLES were calculated using the NOAA READY web-based Hybrid Single-Particle Lagrangian Integrated Trajectory model (HYSPLIT; Stein et al., 2015). The trajectories were driven by the global 0.25° Global Forecast System meteorological dataset and were calculated for arrival heights of 1200 and 1800 m above mean sea level. These heights were selected to compare airflow near the observation-site elevation with airflow in the overlying atmosphere. Because initialization was tied to rainfall onset, the trajectories describe the event-start transport background and were interpreted together with the measured intra-event concentration changes; they do not measure chemical composition along the pathways.

https://doi.org/10.5194/egusphere-2026-6335
Preprint. Discussion started: 6 November 2026
© Author(s) 2026. CC BY 4.0 License.

Hourly ERA5 reanalysis data with a horizontal resolution of 0.25° were used to examine the 925 hPa horizontal wind fields and the vertical distributions of cloud liquid water content and airflow during the representative R1 and R12 events (Hersbach et al., 2020). The 925 hPa fields were used to describe regional low-level airflow, whereas the vertical cross-sections were used to examine airflow and cloud liquid water content over the terrain. The cross-sections were constructed along the southwest–northeast direction for R1 and the southeast–northwest direction for R12. Terrain elevation along each cross-section was obtained from the GEBCO_2026 Grid (GEBCO Bathymetric Compilation Group, 2026). Gridded monthly NO_x emissions were superimposed on the horizontal wind fields to indicate the spatial distribution of potential anthropogenic emission regions

2.6 Near-surface meteorological and turbulence observations

Near-surface air temperature and relative humidity were measured using a temperature–humidity probe and water-vapour density was calculated from the measured air temperature and water-vapour pressure. Precipitation was measured using a rain gauge. Three-dimensional wind components were measured using a CSAT3 sonic anemometer (Campbell Scientific, USA), and turbulent kinetic energy was calculated as

$$TKE = \frac{1}{2}(\sigma_u^2 + \sigma_v^2 + \sigma_w^2), \quad (9)$$

where σu, σv, and σw are the standard deviations of the three wind components. All variables were analysed at 30 min intervals. For R3–R6, rainfall onset was defined as the beginning of the first interval with measurable precipitation. The analysis covered the period from 3 h before rainfall onset to 3 h after rainfall end. Missing values were excluded. These observations describe near-surface meteorological and turbulence conditions and do not constitute a vertical boundary-layer profile.

3 Results

3.1 Chemical context and source-regime classification

The 203 samples from 55 events represented 509.8 mm of precipitation. Event-level measured anion and cation equivalents covaried strongly (ΣAnions = 0.39×ΣCations+ 6.43, R^2 = 0.96; Table S1), while the slope below unity indicates a systematic measured-anion deficit. Similar low slopes occur in several mountain datasets. Five of the six urban-site records compiled in Table S1 had slopes between 0.71 and 1.03, with Kathmandu as the exception (0.44), whereas seven of the nine mountain or remote-mountain records, including ABLES, had slopes ranging from 0.21 to 0.49. The ABLES slope (0.39) was comparable to the 2005–2009 record at Nam Co (0.37), that at Mangdang Mountain in Nanping (0.38), and those at the Nepalese mountain sites of Dhunche, Dimsa, and Gosainkunda (0.43–0.49). Unmeasured bicarbonate, carbonate, or organic anions may contribute, so the regression is treated only as an ionic-consistency diagnostic. Together with the analytical QA/QC described in Sect. 2.2, the consistent event-to-event covariation supports the use of the measured-ion dataset for subsequent analyses of relative ionic composition and variability.

https://doi.org/10.5194/egusphere-2026-6335
Preprint. Discussion started: 6 November 2026
© Author(s) 2026. CC BY 4.0 License.

The VWM concentrations of the nine ions decreased in the order NH_4^+ (23 μeq L^{-1}) > Ca^{2+} (22 μeq L^{-1}) > SO_4^{2-} (14 μeq L^{-1}) > Na^+ (11 μeq L^{-1}) > Cl^- (10 μeq L^{-1}) > K^+ (9 μeq L^{-1}) > NO_3^- (6 μeq L^{-1}) > F^- (4 μeq L^{-1}) = Mg^{2+} (4 μeq L^{-1}) (Table S2). Their sum was 103 μeq L^{-1}. NH_4^+ and Ca^{2+} contributed 22.3 % and 21.4 %, respectively, and together with SO_4^{2-} and Na^+ accounted for 68.0 % of the measured-ion total. Maxima substantially exceeded medians for most ions, showing that the annual summary masks large event-to-event variability. The composition reflects mixed influence. Abundant NH_4^+ is consistent with agricultural and regional inputs, Ca^{2+} with mineral material, and Na^+ and Cl^- with marine transport (Liu et al., 2016; Zhang et al., 2020; Ma et al., 2021; Grider et al., 2023; Paudel Adhikari et al., 2024; Si and Li, 2024). The Na^+/Cl^- equivalent ratio of about 1.2, above the seawater value of 0.86, suggests non-marine Na^+ and/or chloride loss (Keene et al., 1986). Comparison with selected urban, mountain, and regional background sites further defines the chemical setting (Table S3). SO_4^{2-} and NO_3^- at ABLES were generally lower than in the selected urban datasets, while the relative importance of Ca^{2+}, Na^+, and Cl^- was closer to mountain and background precipitation. NH_4^+ nevertheless exceeded several remote-mountain observations, demonstrating continued exposure to agricultural and regional anthropogenic sources. ABLES is therefore a comparatively clean elevated receptor rather than an isolated pristine site (Conrad-Rooney et al., 2023; Hůnová et al., 2024). Figure 1 places ABLES in a global context using Σ8 concentrations, defined here as the sum of eight major ions excluding fluoride, from 323 other precipitation-chemistry sites. These data were compiled primarily from the Cooperative Programme for Monitoring and Evaluation of the Long-range Transmission of Air Pollutants in Europe (EMEP), the National Atmospheric Deposition Program (NADP), and the Acid Deposition Monitoring Network in East Asia (EANET). The ABLES Σ8 value of 99 μeq L^{-1} lay within the global distribution and was not elevated. Within the Chinese subset, it was lower than the Mt. Waliguan Global Atmosphere Watch station and all national background stations included in the comparison. Thus, ABLES combines a relatively low ionic load with frequent cloud occurrence, making it suitable for testing whether a large relative cloud-dominated contribution can emerge without high absolute rainwater concentration.

https://doi.org/10.5194/egusphere-2026-6335
Preprint. Discussion started: 6 November 2026
© Author(s) 2026. CC BY 4.0 License.

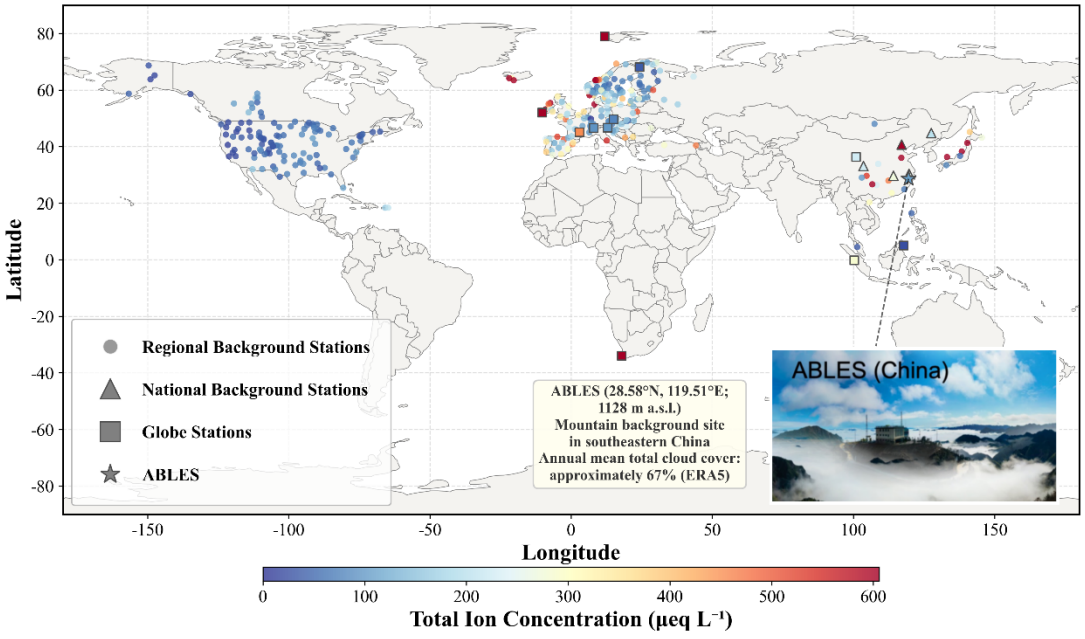


Figure 1: Spatial distribution of Σ8 concentrations in precipitation at ABLES and 323 other sites. Σ8 is the sum of Cl^-, NO_3^-, SO_4^{2-}, NH_4^+, Mg^{2+}, K^+, Ca^{2+}, and Na^+; F^- is excluded so that sites without reported F^- remain comparable. Data were compiled primarily from the EMEP, NADP, and EANET networks, supplemented with published data for selected global and Chinese stations. Colors indicate Σ8 concentrations (μeq L^{-1}), and symbols denote station types. The inset shows ABLES, with annual mean total cloud cover derived from ERA5 reanalysis.

Twelve events contained at least six fractions and were retained for detailed analysis (R1–R12; Table 1). Rainfall depth ranged from 5.8 to 23.6 mm, mean rainfall rate from 2.9 to 44.3 mm h^{-1}, and total measured ionic wet-deposition flux from 17.2 to 87.7 mg m^{-2}. The range spans weak and concentrated rainfall and more than a fivefold difference in ionic loading, providing a diverse event set rather than repetitions of one meteorological condition.

The PCA was suitable (Kaiser–Meyer–Olkin = 0.783; Bartlett $p < 0.001$). Three rotated components explained 80.2 % of variance (Table S5a): secondary inorganic ions and K^+ defined an anthropogenic-related component, Na^+ and Cl^- a marine-related component, and Ca^{2+} a crustal-related component. Pearson correlations support these groupings, yet the component assignments are not mutually exclusive (Table S5b; Yang et al., 2012; Zeng and Han, 2020; Li et al., 2022; Liu et al., 2024; Paudel Adhikari et al., 2024). Among R1–R12, R1–R3 had positive PC1 scores of 0.291–0.336 and comparatively high non-sea-salt sulfate (nss-SO_4^{2-}), identifying them as anthropogenic-type events (Fig. 2). R9–R11 were separated along PC3, with scores of 1.169–2.510, and had elevated nss-Ca^{2+}, identifying a predominant crustal signature. R4–R8 and R12 had weaker anthropogenic and crustal scores and were provisionally grouped as marine type. Non-sea-salt components provided a compositional check. The dataset-specific boundaries in Fig. 2b are visualization aids, not universal thresholds. R1–R3 had elevated nss-SO_4^{2-}, R9–R11 had elevated nss-Ca^{2+}, and most marine-type events remained below both boundaries.

https://doi.org/10.5194/egusphere-2026-6335
Preprint. Discussion started: 6 November 2026
© Author(s) 2026. CC BY 4.0 License.

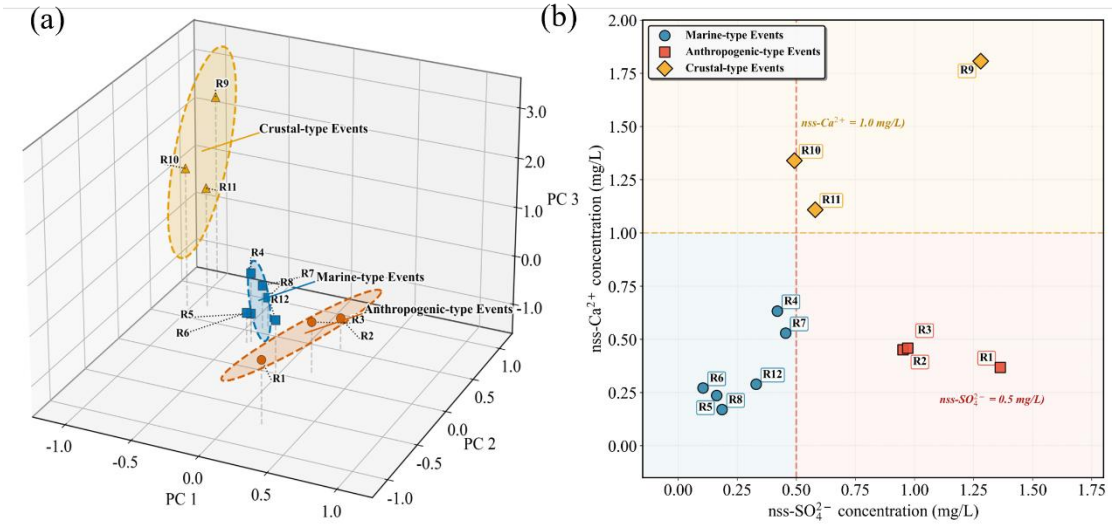


Figure 2: Source-related classification of the 12 sequentially sampled rainfall events at ABLES based on (a) rotated PCA scores and (b) nss-SO_4^{2-} and nss-Ca^{2+} concentrations. Dashed ellipses in (a) are visual guides for the event groups. In (b), the vertical dashed line denotes the dataset-specific nss-SO_4^{2-} boundary of 0.5 mg L^{-1}, whereas the horizontal dashed line denotes the dataset-specific nss-Ca^{2+} boundary of 1.0 mg L^{-1}.

Combining the component scores, correlation structure, and non-sea-salt concentrations yielded three predominant types: anthropogenic (R1–R3), marine (R4–R8 and R12), and crustal (R9–R11). The word type refers to the leading source-related chemical signature, not an exclusive contribution. Mixed sulfate in crustal events and coastal exposure during marine transport are retained as part of the interpretation rather than treated as classification failures (Li et al., 2022).

Table 1: Sampling information, rainfall characteristics, and total ionic wet-deposition fluxes for the 12 sequentially sampled events at ABLES.

Sampling period	Event	Number of fractions	Rainfall depth (mm)	Mean rainfall rate (mm h^{-1})	Total ionic wet-deposition flux (mg m^{-2})
23 April, 17:09–00:34	R1	16	22	2.9	87.7
28 April,	R2	10	10	/	45.5
31 May, 20:09–21:33	R3	6	19.9	14.2	82.3
14 July, 20:22–20:52	R4	7	6.3	12.6	25.8
18 July, 17:41–18:13	R5	8	23.6	44.3	38.2
19 July, 18:33–18:53	R6	9	13.7	41.1	17.2
3 August, 15:48–16:22	R7	6	5.8	10.2	25.7
28 August, 20:07–21:42	R8	9	8.5	5.4	27.8
12 September, 17:06–18:41	R9	9	8.5	5.4	51.4

https://doi.org/10.5194/egusphere-2026-6335
Preprint. Discussion started: 6 November 2026
© Author(s) 2026. CC BY 4.0 License.

Sampling period	Event	Number of fractions	Rainfall depth (mm)	Mean rainfall rate (mm h^{-1})	Total ionic wet-deposition flux (mg m^{-2})
14 September, 17:35–17:59	R10	11	10.7	26.75	36.1
15 September, 21:22–00:00	R11	12	12	4.6	43.1
26 September, 02:17–03:13	R12	11	12	11.9	18.5

3.2 Event-scale sequential evolution

3.2.1 Sequential concentration changes

Across the 12 events, total ion concentration declined with cumulative rainfall, with the largest changes in initial fractions and late rebounds (Fig. 3). Anthropogenic-type events (R1–R3) began at 10.9–13.3 mg L^{-1} and decreased to 4.8–7.8 mg L^{-1} by the third fraction (41.6 %–59.4 %). Secondary inorganic ions contributed 43.3 %–70.7 % of the first-fraction total and dominated the early decrease. Crustal-type events began at 5.4–10.1 mg L^{-1} and decreased by 7.7 %–41.4 %. Their Ca^{2+} share increased from 16.9 %–21.6 % to 41.6 %–57.3 %, although Ca^{2+} decreased in R9, increased in R10, and changed little in R11, indicating relative persistence rather than increasing mineral input. Marine-type events began at 2.4–9.8 mg L^{-1}, showed the widest early decreases (17.1 %–78.2 %), and reached 0.3–3.5 mg L^{-1} in later fractions. Rebounds in R4, R8, and R10 coincided with longer collection times for equal-depth fractions (Fig. S1), but effects of rainfall intensity, cell evolution, and below-cloud replenishment could not be separated (Wang et al., 2021; Audoux et al., 2023b). The event-type contrast is consequently most robust at the level of initial loading and broad compositional evolution: anthropogenic events showed a high secondary-inorganic excess, crustal events showed relative Ca^{2+} persistence, and marine events were lower but heterogeneous. The rebounds caution against treating a single exponential curve as a complete description of event physics and motivate the alternative-baseline test in Sect. 3.4.4.

https://doi.org/10.5194/egusphere-2026-6335
Preprint. Discussion started: 6 November 2026
© Author(s) 2026. CC BY 4.0 License.

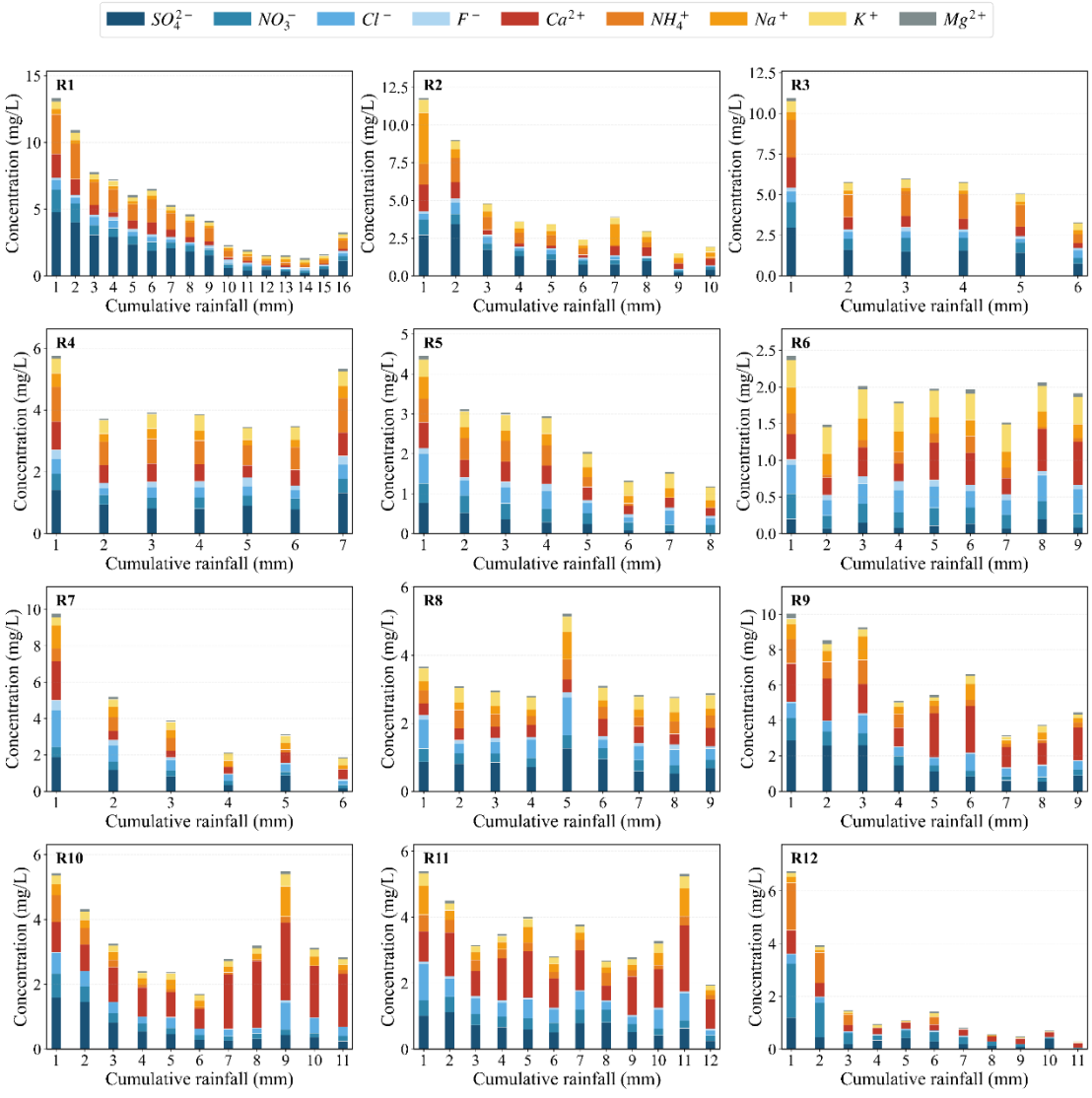


Figure 3: Evolution of major-ion concentrations with cumulative rainfall during the 12 sequentially sampled rainfall events (R1–R12) at ABLES. Each stacked bar represents a sequential rainwater fraction, and the colored segments indicate the concentrations of SO_4^{2-}, NO_3^-, Cl^-, F^-, Ca^{2+}, NH_4^+, Na^+, K^+, and Mg^{2+}. The total bar height represents the sum of the nine measured ions.

3.2.2 Contrast with a remote marine site

To test whether late-stage precipitation at ABLES can approach remote marine loading, final fractions of R6, R7, R8, and R12 were compared with EANET Ogasawara precipitation (Fig. 4). Ogasawara provides a marine reference with different sampling periods and meteorological histories. At Ogasawara, first-day precipitation showed higher and more variable total ion concentrations than precipitation collected on subsequent rainy days. The subsequent-day distribution was used as a reference for low ionic loading under a marine background. The selected ABLES late fractions contained 1.915, 1.868, 2.883, and 0.298

https://doi.org/10.5194/egusphere-2026-6335
Preprint. Discussion started: 6 November 2026
© Author(s) 2026. CC BY 4.0 License.

mg L^{-1} total ions and fell within or near the Ogasawara subsequent-day distribution. Under the sequential-sampling framework, these late fractions are expected to have a smaller relative below-cloud contribution than the initial fractions (Ge et al., 2021; Audoux et al., 2023b). The comparison demonstrates that an inland high-elevation receptor can episodically collect late-stage rainwater with ionic loading comparable to a remote marine site when transport is predominantly marine or coastal. It does not imply that all marine-type events converge to a universal background concentration. Instead, sequential sampling identifies short-lived low-loading states that would be obscured in an event-total sample.

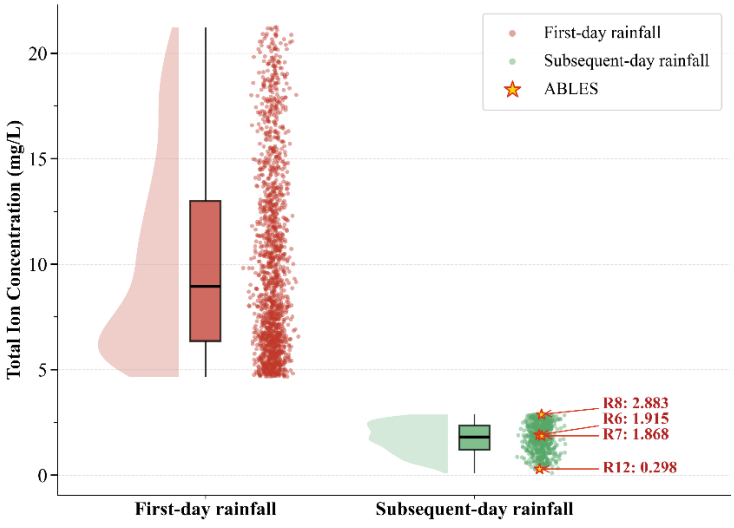


Figure 4: Total ion concentrations in first-day and subsequent-day precipitation at the EANET Ogasawara station and in selected low-concentration late fractions at ABLES (R6, R7, R8, and R12). Half-violin plots, boxplots, and points show distributions, summary statistics, and individual observations.

3.3 Transport and near-surface boundary-layer context

3.3.1 Transport pathways and vertical atmospheric structure

The event-specific differences in rainwater chemistry described above suggest that changes in atmospheric transport may have influenced both the initial ionic composition and its subsequent evolution during rainfall. To examine the regional transport context, 72-h backward trajectories arriving at the Atmospheric Boundary Layer Eco-Environment Shanghuang Observatory (ABLES) at rainfall onset were calculated at 1200 and 1800 m a.s.l. (Fig. S2). The two arrival heights represent transport near the station elevation and within the overlying atmosphere, respectively. For most events, trajectories at the two heights originated from broadly similar sectors. However, clear differences in transport direction and pathway were observed for several events, showing that the event-start transport background was not always the same at the two arrival heights. Initialized at rainfall onset, they test the meteorological plausibility of source-related groupings but neither follow the full event nor apportion chemical mass. R1–R3 approached through different continental or coastal sectors, arguing against one geographical source despite their common secondary-inorganic signature. R9–R11 likewise lacked a common long-range dust pathway;

https://doi.org/10.5194/egusphere-2026-6335
Preprint. Discussion started: 6 November 2026
© Author(s) 2026. CC BY 4.0 License.

315 their Ca^{2+} may reflect regional or local mineral material encountered during transport or final approach. Most marine-type trajectories spent substantial time over adjacent seas or the western North Pacific. Subsequent coastal passage explains why marine Na^{+}–Cl^{-} signatures coexisted with secondary inorganic ions (Ma et al., 2021).

During R1, low-level flow crossed eastern or northeastern regions with elevated anthropogenic emissions, while a 1.2–2.0 km cloud-liquid-water layer coincided with ascent over windward terrain (Fig. 5). The structure is compatible with the initial 320 secondary-inorganic load but does not identify incorporation height. During R12, easterly and southeasterly marine–coastal flow accompanied ascent and enhanced cloud liquid water at approximately 1.2–1.8 km. Coastal passage remains compatible with secondary inorganic ions in this predominantly marine case. Together, the two cases demonstrate that source-regime contrasts at ABLES occurred within different transport and cloud-bearing structures. HYSPLIT and ERA5 diagnose plausible pathways and terrain-related ascent, but neither is a vertical chemical profile. They cannot establish the altitude of pollutant 325 incorporation, cloud-base height, or the quantitative chemical contribution of each level (Paudel Adhikari et al., 2024).

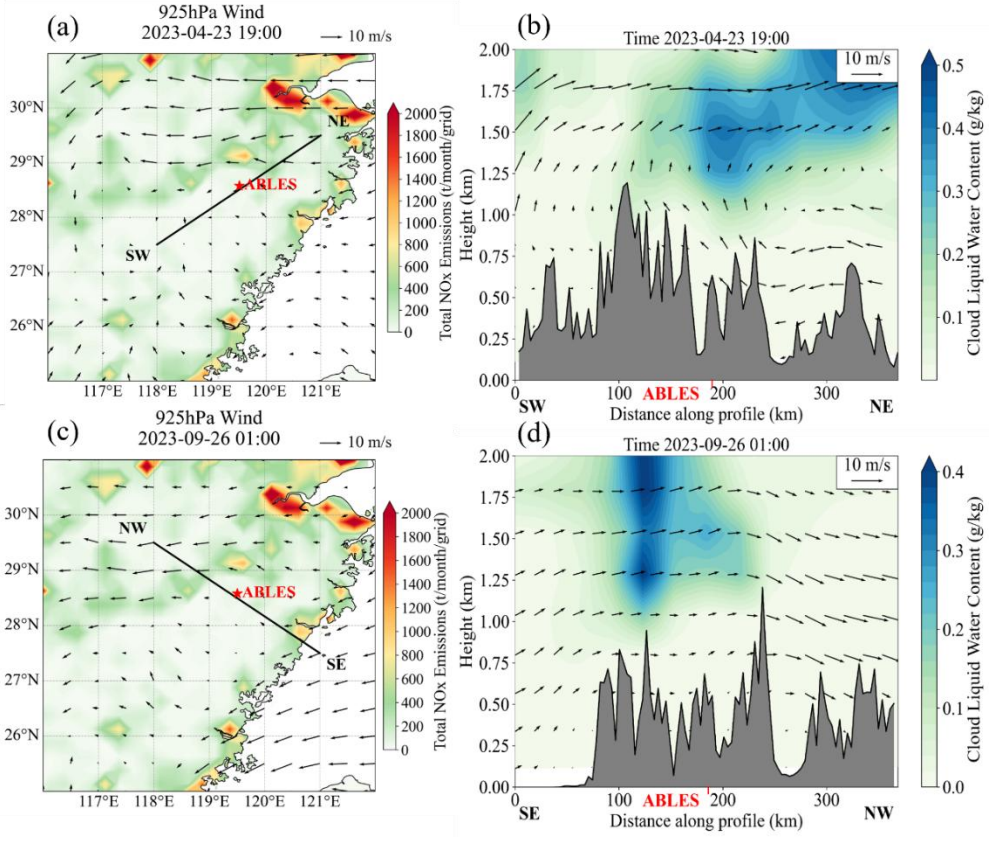


Figure 5: Horizontal transport and vertical atmospheric structure for the contrasting anthropogenic-type event R1 and marine-type event R12. Panels (a) and (b) show R1 at 19:00 on 23 April 2023, and panels (c) and (d) show R12 at 01:00 on 26 September 2023. Panels (a) and (c) show 925 hPa winds and monthly NO_x emissions; panels (b) and (d) show cloud liquid water, terrain, and projected 330 **wind vectors. The red star marks ABLES.**

https://doi.org/10.5194/egusphere-2026-6335
Preprint. Discussion started: 6 November 2026
© Author(s) 2026. CC BY 4.0 License.

3.3.2 Near-surface meteorological context for the early chemical evolution of R3–R6

Figure 6 shows the variations in near-surface meteorological variables during rainfall events R3–R6. All four events were accompanied by decreasing air temperature and increasing turbulent kinetic energy (TKE). Relative to the pre-rainfall periods, mean air temperature decreased by approximately 2.5–3.8 °C, while mean TKE increased from 0.30–1.47 $m^2 s^{-2}$ before rainfall to 2.41–6.96 $m^2 s^{-2}$ during rainfall. These changes demonstrate that the sequential rainwater samples were collected during periods of enhanced near-surface turbulence and marked thermal disturbance. R6 exhibited the largest TKE enhancement and therefore the strongest near-surface dynamical disturbance among the four events. However, these measurements characterize local near-surface conditions and do not resolve the vertical structure of the boundary layer or cloud-level updraughts.

The rainfall amount and water-vapour density differed substantially among the four events. R3, R5, and R6 accumulated 19.9, 23.6, and 13.7 mm of rainfall, respectively, with maximum 30 min accumulations of 12.5, 10.6, and 13.7 mm. These values were substantially higher than those of R4, which accumulated 6.3 mm and had a maximum 30 min accumulation of 4.9 mm. Water-vapour density decreased from 19.68 to 17.13 g m^{-3} during R5 and from 20.36 to 18.19 g m^{-3} during R6. It changed little during R3, decreasing slightly from 18.03 to 17.99 g m^{-3}. In contrast, water-vapour density increased from 17.61 to 17.91 g m^{-3} during R4 and continued to increase after rainfall. Thus, cooling and enhanced turbulence were common to all four events, whereas their near-surface moisture responses were not uniform.

Figure 3 shows pronounced initial decreases in total-ion concentration during R3, R5, and R6. From the first to the second sequential fraction, total-ion concentration decreased from 10.95 to 5.79 mg L^{-1} in R3, from 4.46 to 3.12 mg L^{-1} in R5, and from 2.43 to 1.49 mg L^{-1} in R6, corresponding to decreases of 47.2 %, 30.0 %, and 38.8 %, respectively. Concentrations subsequently remained relatively low and varied less than during the initial rainfall stage, although R3 continued to decrease during its late fractions. The concurrence of these initial chemical decreases with concentrated rainfall, surface cooling, and enhanced TKE shows that the strongest early chemical transitions occurred under markedly disturbed near-surface meteorological conditions. This temporal association is consistent with rapid changes in the amount and composition of soluble material available for below-cloud scavenging, but it does not distinguish among depletion, dilution, horizontal advection, turbulent mixing, and changes in precipitation microphysics. It therefore does not demonstrate that rainfall intensity or turbulence directly caused the concentration decreases, nor does it identify the altitude or pathway through which chemical species were incorporated into precipitation.

The large first-to-second-fraction decreases during R3, R5, and R6 occurred within a small amount of accumulated rainfall. At the nominal sampling resolution of 1 mm, the rapid initial transition was represented by only two adjacent bulk fractions. The measurements therefore captured the pronounced initial concentration decrease but could not determine its precise transition depth or rate of decline. This limitation was particularly important for R3, for which only six fractions were collected and total-ion concentration continued to decrease during the late stage. Its final three fractions may consequently not represent a fully stabilized late-event composition, and the estimated cloud-dominated baseline may be biased high. Such a bias would overestimate the relative in-cloud contribution and correspondingly underestimate the below-cloud contribution for R3.

https://doi.org/10.5194/egusphere-2026-6335
Preprint. Discussion started: 6 November 2026
© Author(s) 2026. CC BY 4.0 License.

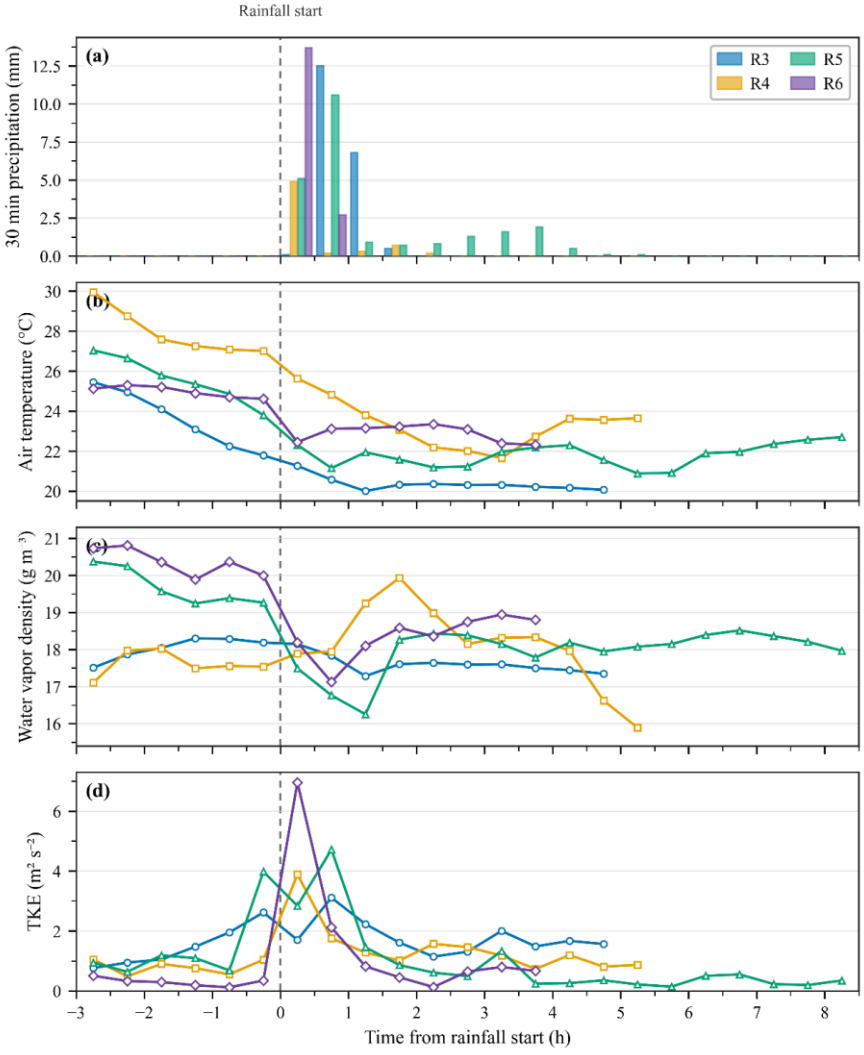


Figure 6: Near-surface conditions during R3–R6. (a) Thirty-minute precipitation, (b) air temperature, (c) water-vapour density, and (d) turbulent kinetic energy (TKE), plotted relative to rainfall onset. The dashed line marks rainfall onset (0 h).

3.4 Estimated in-cloud scavenging contributions

3.4.1 Sequential SO_4^{2-} evolution from urban pollution to global mountain levels

Sequential SO_4^{2-} measurements at ABLES were compared with same-method observations from Beijing, Rizhao, and Wuhan (Fig. 7a; Yao et al., 2024). Median first-fraction concentrations were 1.50 mg L^{-1} at ABLES, compared with 14.67, 9.04, and 4.92 mg L^{-1} at the three urban sites, respectively. By the third fraction, they had declined to 0.81, 7.07, 2.56, and 2.44 mg L^{-1}, and subsequent concentrations at ABLES generally remained below 1 mg L^{-1}. The fitted curves reinforce this contrast. In $y = Ae^{-kx} + C$, the initial-excess parameter A was 1.46 mg L^{-1} at ABLES but 6.49–43.13 mg L^{-1} at the urban sites, while C was

https://doi.org/10.5194/egusphere-2026-6335
Preprint. Discussion started: 6 November 2026
© Author(s) 2026. CC BY 4.0 License.

only 0.32 mg L^{-1} at ABLES, approximately one-seventh to one-eleventh of the urban asymptotes. The lower k at ABLES (0.27 mm^{-1} versus 0.48–2.01 mm^{-1}) describes a gradual decline from an already low initial concentration rather than weak scavenging. The same-method comparison therefore shows that ABLES had both a smaller sulfate burden available for additional below-cloud removal and a much lower late-event level. A large relative in-cloud contribution can consequently coexist with low absolute sulfate concentration.

This low late-event level represents a marked departure from the sulfate-rich mountain-cloud environment documented in China during the coal-driven acid-rain period. Direct cloud-water SO_4^{2-} concentrations reached 51.1 mg L^{-1} at Mt. Tai during 2007–2008 and 18.8 mg L^{-1} at Mt. Heng in 2009, compared with approximately 10.6 mg L^{-1} at Whiteface Mountain in 2006 and about 3.5–27 mg L^{-1} at reported European mountain sites (Aleksic et al., 2009; Guo et al., 2012; Li et al., 2017). The fitted ABLES baseline of 0.32 mg L^{-1} and final-fraction median of 0.49 mg L^{-1} were therefore one to two orders of magnitude lower than these historical mountain observations. Whiteface measurements from 2010–2017 further showed a mean of 3.55 mg L^{-1} under low-smoke conditions, with a 10th percentile of approximately 0.29 mg L^{-1} (Lee et al., 2022 ; Lawrence et al., 2023). Thus, the cloud-dominated late-event signature at ABLES reached the lower range of recent international mountain observations. Because late-event rainwater is not equivalent to directly collected cloud water and cloud-water concentrations depend on liquid water content, this comparison does not establish that ABLES clouds were intrinsically cleaner. It instead provides rare event-resolved evidence that sulfate in an elevated cloud–precipitation system in southeastern China has entered a globally low concentration regime, consistent with the broader effects of China's sulfur-emission controls extending beyond surface air (Liu et al., 2020).

3.4.2 Comparison of in-cloud scavenging contributions across different environments

Estimated NO_3^-, SO_4^{2-}, and NH_4^+ contributions were compared with published urban and remote values (Fig. 7b; Chatterjee et al., 2010; Aikawa et al., 2014; Kajino and Aikawa, 2015; Ge et al., 2016, 2021; Xu et al., 2017; Bayramoğlu Karşı et al., 2018; Monteiro et al., 2021; Ryu and Min, 2022; Zou et al., 2022; Audoux et al., 2023b; Yao et al., 2024). ABLES medians were 58.4 %, 51.1 %, and 49.2 %, with event ranges of 23.3 %–81.9 %, 29.8 %–79.5 %, and 19.7 %–80.5 %, respectively. The ABLES medians exceeded compiled urban observational and model medians but overlapped remote ranges. The comparison reflects broad environmental differences across studies with different methods. Together with Fig. 7a, this pattern suggests a larger relative late-stage contribution where additional below-cloud material is limited.

This pattern is consistent with model studies indicating that below-cloud scavenging is generally more important in the polluted lower atmosphere, whereas the relative importance of in-cloud scavenging increases in elevated or remote environments (Grythe et al., 2017; Kim et al., 2021; Jones et al., 2022; Ryu and Min, 2022). Because the compiled values were obtained using different observational designs, model frameworks, and calculation procedures, they are used here only to characterize broad environmental contrasts. It is worthy to note that the wide ranges observed at ABLES further show that in-cloud scavenging was not uniformly dominant but varied among chemical species and rainfall events.

https://doi.org/10.5194/egusphere-2026-6335
Preprint. Discussion started: 6 November 2026
© Author(s) 2026. CC BY 4.0 License.

3.4.3 Event- and ion-specific variability in in-cloud scavenging contributions

Estimated in-cloud contributions varied substantially among events and ions (Fig. 7c). For anthropogenic-type events R1–R3, median estimates for SO_4^{2-}, NO_3^-, and NH_4^+ were 34.5 %, 44.8 %, and 20.5 %, respectively. Their high initial loads and pronounced early decreases corresponded, within the sequential-sampling framework, to larger early concentration excesses assigned to the below-cloud component, rather than directly measured removal fluxes. Marine-type medians were 60.3 % for SO_4^{2-}, 61.3 % for NO_3^-, 53.4 % for NH_4^+, 85.1 % for Cl^-, and 85.5 % for Na^+. R4–R6 showed relatively high estimates for most ions, whereas R7, R8, and R12 showed more balanced partitioning of secondary inorganic ions. R12 retained high estimated contributions for Cl^-, Na^+, Mg^{2+}, and Ca^{2+} but only moderate values for SO_4^{2-}, NO_3^-, and NH_4^+, demonstrating ion-specific behaviour within a single marine-type event. For crustal-type events R9–R11, estimated Ca^{2+} contributions ranged from 71.9 % to 95.0 % (median: 94.8 %), and Mg^{2+} contributions from 51.9 % to 86.0 % (median: 83.9 %). Estimates for secondary inorganic ions were low in R9 but higher in R10 and R11. Trajectory differences provide meteorological context but cannot locate chemical incorporation. Overall, chemical type was associated with, but did not uniquely determine, the estimated partitioning; variability was event- and ion-specific.

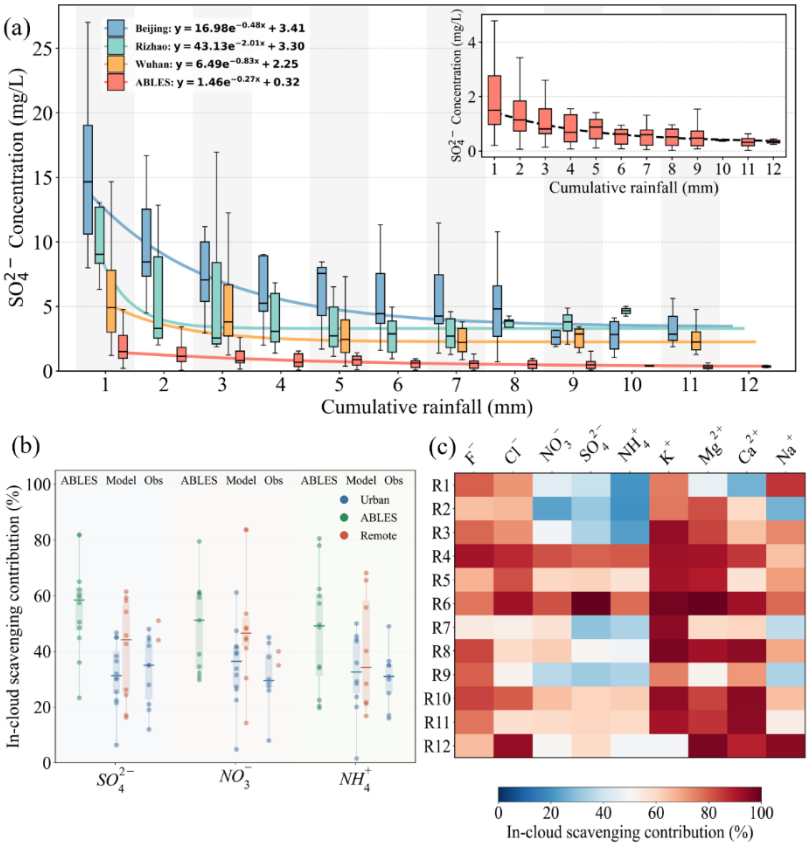


Figure 7: Sequential SO_4^{2-} evolution and estimated in-cloud contributions at ABLES. (a) SO_4^{2-} concentrations and exponential fits at ABLES, Beijing, Rizhao, and Wuhan; (b) estimated contributions of SO_4^{2-}, NO_3^-, and NH_4^+ compared with published urban and remote results; and (c) event-specific estimates for nine ions during R1–R12. Sources for panel (b) are listed in Sect. 3.4.2.

https://doi.org/10.5194/egusphere-2026-6335
Preprint. Discussion started: 6 November 2026
© Author(s) 2026. CC BY 4.0 License.

3.4.4 Robustness of the partition estimates

The across-event median sequential concentration profiles of SO_4^{2-}, NO_3^-, NH_4^+, Na^+, and Cl^- were described using exponential decay functions (Table 2). Across the five ions, R^2 ranged from 0.70 to 0.86 and RMSE ranged from 0.032 to 0.098 mg L^{-1}. Mean residuals were small (−0.029 to 0.001 mg L^{-1}), indicating little systematic signed bias in the fitted profiles. SO_4^{2-} had the largest RMSE, whereas NO_3^- had the smallest. Fitted asymptotic baselines for SO_4^{2-}, NO_3^-, NH_4^+, Na^+, and Cl^- were 0.320, 0.210, 0.230, 0.200, and 0.300 mg L^{-1}; event-specific final-three medians were 0.49, 0.20, 0.17, 0.24, and 0.33 mg L^{-1}. Sensitivity was closest for nitrate and largest for sulfate, with no uniform directional shift. The fitted asymptote was retained as the primary baseline for these five ions, while final-three-fraction means were retained as the alternative and as the fallback for the remaining ions (Table S4). The comparison supports qualitative conclusions that are stable across the two representations, such as the low late-stage sulfate concentration, but cautions against treating individual event percentages as exact process measurements.

Table 2: Exponential-fit diagnostics and comparison of fitted asymptotic and event-specific final-three-fraction concentration baselines for the five ions with acceptable across-event median fits.

Ion	Fitted equation	R^2	RMSE (mg L^{-1})	Mean signed residual (mg L^{-1})	Fitted asymptote C (mg L^{-1})	Median of event-specific final-three means (mg L^{-1})
SO_4^{2-}	$y = 0.32 + 1.46e^{-0.27x}$	0.70	0.098	−0.004	0.320	0.49
NO_3^-	$y = 0.21 + 0.64e^{-0.39x}$	0.86	0.032	−0.014	0.210	0.20
NH_4^+	$y = 0.23 + 1.29e^{-0.49x}$	0.79	0.062	−0.029	0.230	0.17
Na^+	$y = 0.20 + 0.59e^{-0.88x}$	0.70	0.040	0.001	0.200	0.24
Cl^-	$y = 0.30 + 0.68e^{-0.25x}$	0.85	0.058	−0.011	0.300	0.33

Note: x denotes cumulative rainfall depth (mm), and y denotes ion concentration (mg L^{-1}).

4 Discussion

4.1 Meaning of a high estimated in-cloud contribution at an elevated receptor

The sequential partition separates a late-stage baseline from the early concentration excess acquired during the event. At ABLES, estimated in-cloud fractions for sulfate, nitrate, and ammonium exceeded compiled urban medians but remained within remote-environment ranges. The first-order explanation is not necessarily enhanced cloud-water concentration. An elevated receptor has a shorter and often cleaner sub-cloud column than a polluted lowland site, so the additional amount available for below-cloud collection can be small relative to the material already associated with precipitating cloud (Grythe et al., 2017; Kim et al., 2021; Jones et al., 2022; Ryu and Min, 2022). The resulting ratio can be high even when both

https://doi.org/10.5194/egusphere-2026-6335
Preprint. Discussion started: 6 November 2026
© Author(s) 2026. CC BY 4.0 License.

components are modest in absolute concentration. Sulfate provides the clearest demonstration. ABLES had much lower first-fraction sulfate than Beijing, Rizhao, and Wuhan and a fitted asymptote only one-seventh to one-eleventh of the urban values. A large relative baseline contribution at ABLES therefore coexists with low sulfate throughout the event. The physically transferable conclusion is that relative process partition and absolute ionic loading answer different questions: the former describes how event deposition is divided under the adopted baseline, while the latter describes the amount delivered. Neither by itself measures cloud-water composition. This distinction helps reconcile apparently high in-cloud fractions at clean or elevated sites with modest chemical loading. It also prevents a percentage from one environment being treated as a process rate equivalent to that from another. Comparisons are most informative when initial concentration, late-stage concentration, event deposition, and relative partition are reported together. The ABLES observations supply that combined benchmark for a monsoon-influenced inland mountain receptor.

The implication for process evaluation is specific. Reproducing an annual wet-deposition total is insufficient if the early concentration excess or late-stage baseline is wrong, because compensating errors can yield the correct integral. Conversely, agreement in a relative fraction does not ensure agreement in deposited mass. The observed sequence offers four linked constraints: starting concentration, decline with accumulated rainfall, baseline magnitude, and ion-specific deposition fraction. Evaluation against all four would better distinguish errors in atmospheric loading from errors in wet-removal treatment. The two-baseline comparison clarifies which part of this benchmark is most stable. Nitrate showed close agreement between the exponential asymptote and final-three-fraction summary, whereas sulfate was more sensitive. This difference is scientifically relevant because it prevents all ions from being assigned the same methodological confidence. A framework that reproduces nitrate partition but not sulfate evolution may therefore point to species-specific differences in precursor supply, particle association, or aqueous processing rather than a uniform precipitation bias. The present data identify that diagnostic opportunity without resolving the underlying process uniquely.

Cross-environment comparison introduces additional structural uncertainty. Urban records combine higher precursor abundance, longer sub-cloud paths, and different precipitation climatology, whereas remote observations may differ in sampling duration and analytical coverage. The compiled medians therefore cannot isolate elevation from pollution level or microphysics. Their value is that they define the range of observed behaviour. ABLES occupies a distinctive part of that range: remote-like relative contributions paired with measurable regional anthropogenic influence and low absolute sulfate. This combination is the evidence for a mountain-receptor transition regime, not proof that elevation alone causes the observed partition.

4.2 Transport context and source-related chemical signatures

Source-related event types differed in both the material present at rainfall onset and its evolution. Anthropogenic-type events began with a strong secondary-inorganic excess and yielded larger estimated below-cloud fractions. Marine-type events generally began at lower concentration and retained large late-stage fractions for sodium and chloride, while crustal-type events

https://doi.org/10.5194/egusphere-2026-6335
Preprint. Discussion started: 6 November 2026
© Author(s) 2026. CC BY 4.0 License.

showed persistence of calcium relative to sulfate, nitrate, and ammonium. These contrasts indicate that source composition sets the chemical reservoir on which rainfall acts.

Transport history modifies that reservoir. The marine cases show that oceanic pathways do not produce chemically pure sea-salt precipitation: coastal passage can add secondary inorganic or mineral material before arrival. Similarly, a crustal chemical signature need not originate from a single distant dust region. The multi-height trajectories show different histories near the station and aloft for several events, and the R1/R12 cross-sections show terrain-related ascent toward cloud-bearing layers. These diagnostics make the observed chemical contrasts physically plausible, while their limitations prohibit quantitative vertical attribution. The R3–R6 near-surface observations add a second line of contextual evidence. Large initial concentration decreases coincided with concentrated rainfall, cooling, and enhanced turbulence in R3, R5, and R6, whereas R4 had weaker rainfall and a different moisture response. This co-variation supports rapid event evolution but cannot show whether ions were collected from a near-surface reservoir, incorporated aloft, or altered by microphysical dilution. Direct chemical profiles, cloud-base observations, and finer sequential sampling would be required to separate those pathways.

The substantial variability within each source group is itself a key result. Source label alone cannot predict wet-scavenging partition because event structure, rainfall history, vertical transport, and ion properties interact. A useful future framework should evaluate individual events and species rather than assign one fixed in-cloud fraction to a broad transport regime. Ion behaviour provides clues to the competing controls. Secondary inorganic ions were prominent in the anthropogenic early excess, sea-salt ions retained large baseline fractions in several marine events, and calcium persisted in crustal cases. These contrasts may reflect differences in vertical distribution, particle size, hygroscopicity, and aqueous processing, but the present observations do not separate them. The appropriate mechanistic inference is therefore a set of testable ion-specific hypotheses, not a closed causal explanation. The mountain setting makes vertical separation particularly plausible but also difficult to verify. Air sampled at station height may have a different history from cloud-bearing air above the ridge, and the precipitating column can change as cells cross complex terrain. Similar trajectories at two arrival heights support a relatively coherent transport sector, whereas divergent trajectories identify conditions in which mixed histories are likely. Neither case proves where ions entered hydrometeors. Direct aerosol and gas profiles below and above cloud base would be needed to distinguish pre-cloud transport, in-cloud uptake, and collection during descent.

4.3 Methodological scope and limitations

Several limitations define the scope of the inference. First, the late-stage baseline is derived from rainwater rather than measured cloud water. Air-mass transitions, changing rainfall intensity or drop spectra, evaporation, and replenishment below cloud can violate exponential decay. The R4, R8, and R10 rebounds demonstrate that departures occur. R^2, RMSE, and mean signed residual assess fitted concentration profiles, while the final-three comparison tests structural baseline sensitivity; none is a direct probability distribution for the process fraction. The baseline uncertainty is therefore partly identifiable and partly irreducible with the present dataset. Agreement between two baselines increases confidence that the late concentration level is not an artefact of one fitting choice, but agreement cannot validate the underlying cloud-dominated interpretation. Independent

https://doi.org/10.5194/egusphere-2026-6335
Preprint. Discussion started: 6 November 2026
© Author(s) 2026. CC BY 4.0 License.

cloud-water samples or simultaneous vertical chemical observations are required for that test. Reporting both forms of uncertainty prevents numerical fit precision from being confused with physical identifiability. Second, only 12 of 55 events contained at least six sequential fractions, and the three source groups are small and unequal. The classification is useful for organizing contrasts but does not support causal population-level differences among regimes. The 1 mm collection increment also undersamples the sharpest initial transition, particularly for R3, where only six fractions were available and the concentration continued to decline late in the event. Third, the chemical analysis is restricted to nine inorganic ions. The anion–cation slope indicates that unmeasured bicarbonate, carbonate, organic anions, or acidity may matter, and conductivity was not available as an independent check. Concurrent blanks, blank subtraction, replicate precision below 5 %, certified materials, and the ionic-consistency analysis support the reported measurements but cannot recover unmeasured species. Finally, HYSPLIT, ERA5, and near-surface observations constrain transport and meteorological context, not vertical chemical distributions or incorporation altitude. Within these bounds, sequential sampling reveals information unavailable from bulk precipitation: the secondary-inorganic early excess, relative calcium persistence, occasional low-loading marine late fractions, and ion-dependent baseline sensitivity. These features provide a benchmark for evaluating whether monitoring and wet-removal frameworks reproduce both absolute concentration and event evolution. The term cloud-dominated precipitation signature remains essential because the late fraction is not direct cloud water.

This benchmark also has implications for network design. A high-elevation station can appear chemically clean in monthly or event-mean data while still recording substantial early anthropogenic influence during selected events. Pairing routine deposition totals with targeted sequential sampling would retain long-term comparability and add process resolution during representative transport regimes. Such a nested strategy is more feasible than direct cloud-water sampling at every site and can identify events that warrant intensive vertical observations. Representativeness should be evaluated at several levels. The 55-event dataset supports the annual chemical setting and multivariate source patterns, the 12 long events support sequential comparisons, and only R3–R6 support statements involving the co-located near-surface observations. Conclusions should not be transferred from one evidence tier to another. This hierarchy also suggests a sampling design for future work: broad routine coverage to establish frequency, dense sequential sampling to resolve transitions, and a smaller set of vertically instrumented intensive periods to test mechanism. The findings are most applicable to elevated inland receptors that experience frequent cloud and alternating continental–marine transport. Generalization to polluted lowlands, arid mountains, snow-dominated precipitation, or convective regimes with different microphysics requires additional evidence. Even at ABLES, the present record represents one observation year and emphasizes events long enough to yield at least six fractions; short events may have different chemistry and partition behaviour. Future campaigns should combine sub-millimetre sampling during the first rainfall, sufficient late-event fractions, direct cloud-water collection where feasible, cloud-base and vertical remote sensing, and simultaneous aerosol and gas measurements. Repeated observations across seasons and multiple elevations would test whether the low absolute loading–high relative fraction relationship persists. These measurements would also allow the contextual transport evidence used here to be replaced by direct constraints on the altitude, timing, and chemical form of incorporation.

https://doi.org/10.5194/egusphere-2026-6335
Preprint. Discussion started: 6 November 2026
© Author(s) 2026. CC BY 4.0 License.

5 Conclusions

Sequential rainwater sampling at ABLES revealed event-scale chemical evolution that is obscured by event-integrated measurements. Across 55 events, ionic loads were low relative to urban precipitation, yet the record retained distinct anthropogenic, marine, and mineral influences. Among the 12 sequentially sampled events, anthropogenic-type events had the highest initial concentrations and strongest early decreases, dominated by sulfate, nitrate, and ammonium; marine-type events were lower but more variable; and crustal-type events showed relative Ca^{2+} persistence. Selected late fractions from marine events were within or near the low-concentration subsequent-day distribution at Ogasawara, showing that ABLES alternated among chemically distinct event states rather than representing a uniformly clean background.

Fitted asymptotes were used for ions with acceptable across-event median fits, and each event's final-three-fraction mean for the others. Median estimated in-cloud contributions were 51.1 % for SO_4^{2-}, 58.4 % for NO_3^-, and 49.2 % for NH_4^+; individual estimates exceeded 80 %, and Ca^{2+} reached 95.0 % in one crustal event. Comparison with Beijing, Rizhao, and Wuhan showed that ABLES combined a high relative cloud-dominated contribution with a fitted late-event SO_4^{2-} baseline of only 0.32 mg L^{-1}, a pattern consistent with little additional sulfate being available for below-cloud removal. More importantly, this baseline and the final-three-fraction median of 0.49 mg L^{-1} were one to two orders of magnitude below historical Chinese mountain cloud-water observations and reached the lower range of recent global mountain records, providing rare event-resolved evidence consistent with the effects of sulfur-emission controls extending beyond surface air. Because late-event rainwater is not direct cloud water, the comparison does not demonstrate intrinsically low cloud-water concentrations or stronger absolute in-cloud scavenging; relative contribution, absolute loading, and environmental setting must therefore be reported together.

Transport pathways provided context for, but did not uniquely determine, the event- and ion-specific partitioning. Marine and coastal pathways coincided with lower loading and sea-salt-rich signatures, whereas continental exposure coincided with secondary inorganic enrichment. For R3–R6, concentrated rainfall, cooling, enhanced near-surface turbulence, and rapid initial concentration decreases co-occurred, but these observations neither locate chemical incorporation nor establish causality.

The estimates remain limited by the empirical baseline, 1 mm sampling resolution with small and unequal event groups, event rebounds, and the absence of direct cloud-water, cloud-base, vertical-chemistry measurements. They should therefore be treated as event-resolved observational constraints rather than exact process fractions or universal constants. Sequential sampling nevertheless provides a benchmark for testing whether monitoring and wet-removal frameworks reproduce both the early concentration excess and late-event baseline, rather than only event-total deposition. Coordinated observations across seasons and elevations are required to determine whether the low-loading–high-relative-contribution relationship is a general mountain feature or specific to ABLES.

https://doi.org/10.5194/egusphere-2026-6335
Preprint. Discussion started: 6 November 2026
© Author(s) 2026. CC BY 4.0 License.

Data availability

To request the observed data for scientific research purposes, please contact Baozhu Ge at the Institute of Atmospheric Physics, Chinese Academy of Sciences, via email (gebz@mail.iap.ac.cn).

Author contribution

YC, BG, FL, and ZW designed the overall study framework and wrote the manuscript. NL, LD, XP, and XC assisted with data processing. LY, JX, YS, and LL contributed to the interpretation and discussion of the scientific results. All co-authors contributed to this work.

Competing interests

The authors declare that they have no conflict of interest.

Acknowledgements

We gratefully acknowledge the European Centre for Medium-Range Weather Forecasts (ECMWF) and the Copernicus Climate Change Service (C3S) for providing the ERA5 reanalysis data. We also acknowledge the Acid Deposition Monitoring Network in East Asia (EANET), the National Atmospheric Deposition Program (NADP), and the Cooperative Programme for Monitoring and Evaluation of the Long-range Transmission of Air Pollutants in Europe (EMEP) for making their observational data publicly available. We sincerely thank all participating institutions and monitoring personnel for their contributions to data collection, quality assurance, and data management.

Financial support

This work was supported by the National Natural Science Foundation of China (Nos. 42122049 and 42377104)

References

Aikawa, M. and Hiraki, T.: Washout/rainout contribution in wet deposition estimated by 0.5 mm precipitation sampling/analysis, Atmos. Environ., 43, 4935–4939, https://doi.org/10.1016/j.atmosenv.2009.07.057, 2009.

Aikawa, M., Kajino, M., Hiraki, T., and Mukai, H.: The contribution of site to washout and rainout: Precipitation chemistry based on sample analysis from 0.5 mm precipitation increments and numerical simulation, Atmos. Environ., 95, 165–174, https://doi.org/10.1016/j.atmosenv.2014.06.015, 2014.

https://doi.org/10.5194/egusphere-2026-6335
Preprint. Discussion started: 6 November 2026
© Author(s) 2026. CC BY 4.0 License.

Aleksic, N., Roy, K., Sistla, G., Dukett, J., Houck, N., and Casson, P.: Analysis of cloud and precipitation chemistry at Whiteface Mountain, NY, Atmos. Environ., 43, 2709–2716, https://doi.org/10.1016/j.atmosenv.2009.02.053, 2009.

Audoux, T., Laurent, B., Chevaillier, S., Féron, A., Pangui, E., Maisonneuve, F., Desboeufs, K., Triquet, S., Noyalet, G., Lauret, O., and Huet, F.: Automatic sequential rain sampling to study atmospheric particulate and dissolved wet deposition, Atmos. Environ., 295, 119561, https://doi.org/10.1016/j.atmosenv.2022.119561, 2023a.

Audoux, T., Laurent, B., Desboeufs, K., Noyalet, G., Maisonneuve, F., Lauret, O., and Chevaillier, S.: Intra-event evolution of elemental and ionic concentrations in wet deposition in an urban environment, Atmos. Chem. Phys., 23, 13485–13503, https://doi.org/10.5194/acp-23-13485-2023, 2023b.

Balestrini, R., Diémoz, H., Freppaz, M., Delconte, C. A., Caschetto, M., and Matiatos, I.: Nitrogen atmospheric deposition in a high-altitude Alpine environment: A chemical and isotopic approach to investigate the influence from anthropized areas, Atmos. Environ., 328, 120513, https://doi.org/10.1016/j.atmosenv.2024.120513, 2024.

Bayramoğlu Karşı, M. B., Yenisoy-Karakaş, S., and Karakaş, D.: Investigation of washout and rainout processes in sequential rain samples, Atmos. Environ., 190, 53–64, https://doi.org/10.1016/j.atmosenv.2018.07.018, 2018.

Berberler, E., Gemici, B. T., Ucun Özel, H., Demir, T., and Karakaş, D.: Source identification of water-insoluble single particulate matters in rain sequences, Atmos. Pollut. Res., 13, 101499, https://doi.org/10.1016/j.apr.2022.101499, 2022.

Chatterjee, A., Jayaraman, A., Rao, T. N., and Raha, S.: In-cloud and below-cloud scavenging of aerosol ionic species over a tropical rural atmosphere in India, J. Atmos. Chem., 66, 27–40, https://doi.org/10.1007/s10874-011-9190-5, 2010.

Cheng, I., Al Mamun, A., and Zhang, L.: A synthesis review on atmospheric wet deposition of particulate elements: Scavenging ratios, solubility, and flux measurements, Environ. Rev., 29, 340–353, https://doi.org/10.1139/er-2020-0118, 2021.

Conrad-Rooney, E., Gewirtzman, J., Pappas, Y., Pasquarella, V. J., Hutyra, L. R., and Templer, P. H.: Atmospheric wet deposition in urban and suburban sites across the United States, Atmos. Environ., 305, 119783, https://doi.org/10.1016/j.atmosenv.2023.119783, 2023.

Ge, B., Wang, Z., Gbaguidi, A. E., and Zhang, Q.: Source identification of acid rain arising over Northeast China: Observed evidence and model simulation, Aerosol Air Qual. Res., 16, 1366–1377, https://doi.org/10.4209/aaqr.2015.05.0294, 2016.

Ge, B., Xu, D., Wild, O., Yao, X., Wang, J., Chen, X., Tan, Q., Pan, X., and Wang, Z.: Inter-annual variations of wet deposition in Beijing from 2014–2017: Implications of below-cloud scavenging of inorganic aerosols, Atmos. Chem. Phys., 21, 9441–9454, https://doi.org/10.5194/acp-21-9441-2021, 2021.

GEBCO Bathymetric Compilation Group: The GEBCO_2026 Grid – a continuous terrain model for oceans and land at 15 arc-second intervals, NERC EDS British Oceanographic Data Centre NOC [data set], https://doi.org/10.5285/4f68d5c7-45eb-f999-e063-7086abc036fa, 2026.

Grider, A., Ponette-González, A., and Heindel, R.: Calcium and ammonium now control the pH of wet and bulk deposition in Ohio, U.S., Atmos. Environ., 310, 119986, https://doi.org/10.1016/j.atmosenv.2023.119986, 2023.

https://doi.org/10.5194/egusphere-2026-6335
Preprint. Discussion started: 6 November 2026
© Author(s) 2026. CC BY 4.0 License.

Grythe, H., Kristiansen, N. I., Groot Zwaaftink, C. D., Eckhardt, S., Ström, J., Tunved, P., Krejci, R., and Stohl, A.: A new aerosol wet removal scheme for the Lagrangian particle model FLEXPART v10, Geosci. Model Dev., 10, 1447–1466, https://doi.org/10.5194/gmd-10-1447-2017, 2017.

Guo, J., Wang, Y., Shen, X., Wang, Z., Lee, T., Wang, X., Li, P., Sun, M., Collett, J. L., Wang, W., and Wang, T.: Characterization of cloud water chemistry at Mount Tai, China: Seasonal variation, anthropogenic impact, and cloud processing, Atmos. Environ., 60, 467–476, https://doi.org/10.1016/j.atmosenv.2012.07.016, 2012.

Hersbach, H., Bell, B., Berrisford, P., Hirahara, S., Horányi, A., Muñoz-Sabater, J., Nicolas, J., Peubey, C., Radu, R., Schepers, D., Simmons, A., Soci, C., Abdalla, S., Abellan, X., Balsamo, G., Bechtold, P., Biavati, G., Bidlot, J., Bonavita, M., De Chiara, G., Dahlgren, P., Dee, D., Diamantakis, M., Dragani, R., Flemming, J., Forbes, R., Fuentes, M., Geer, A., Haimberger, L., Healy, S., Hogan, R. J., Hólm, E., Janisková, M., Keeley, S., Laloyaux, P., Lopez, P., Lupu, C., Radnoti, G., de Rosnay, P., Rozum, I., Vamborg, F., Villaume, S., and Thépaut, J.-N.: The ERA5 global reanalysis, Q. J. Roy. Meteor. Soc., 146, 1999–2049, https://doi.org/10.1002/qj.3803, 2020.

Hůnová, I., Brabec, M., and Malý, M.: Major ions in Central European precipitation—Insight into changes in NO_3^-/SO_4^{2-}, NH_4^+/NO_3^- and NH_4^+/SO_4^{2-} ratios over the last four decades, Chemosphere, 349, 140986, https://doi.org/10.1016/j.chemosphere.2023.140986, 2024.

Jones, A. C., Hill, A., Hemmings, J., Lemaitre, P., Quérel, A., Ryder, C. L., and Woodward, S.: Below-cloud scavenging of aerosol by rain: A review of numerical modelling approaches and sensitivity simulations with mineral dust in the Met Office's Unified Model, Atmos. Chem. Phys., 22, 11381–11407, https://doi.org/10.5194/acp-22-11381-2022, 2022.

Kajino, M. and Aikawa, M.: A model validation study of the washout/rainout contribution of sulfate and nitrate in wet deposition compared with precipitation chemistry data in Japan, Atmos. Environ., 117, 124–134, https://doi.org/10.1016/j.atmosenv.2015.06.042, 2015.

Keene, W. C., Pszenny, A. A. P., Galloway, J. N., and Hawley, M. E.: Sea-salt corrections and interpretation of constituent ratios in marine precipitation, J. Geophys. Res.-Atmos., 91, 6647–6658, https://doi.org/10.1029/JD091iD06p06647, 1986.

Kim, K. D., Lee, S., Kim, J.-J., Lee, S.-H., Lee, D., Lee, J.-B., Choi, J.-Y., and Kim, M. J.: Effect of wet deposition on secondary inorganic aerosols using an urban-scale air quality model, Atmosphere, 12, 168, https://doi.org/10.3390/atmos12020168, 2021.

Kok, L., van Zyl, P. G., Beukes, J. P., Burger, R. P., Ellis, S. M., Josipovic, M., Jaars, K., Vakkari, V., Laakso, L., and Kulmala, M.: Factors governing the chemical composition of rain at a regional site in South Africa, Atmos. Environ., 318, 120246, https://doi.org/10.1016/j.atmosenv.2023.120246, 2024.

Lawrence, C. E., Casson, P., Brandt, R., Schwab, J. J., Dukett, J. E., Snyder, P., Yerger, E., Kelting, D., VandenBoer, T. C., and Lance, S.: Long-term monitoring of cloud water chemistry at Whiteface Mountain: The emergence of a new chemical regime, Atmos. Chem. Phys., 23, 1619–1639, https://doi.org/10.5194/acp-23-1619-2023, 2023.

https://doi.org/10.5194/egusphere-2026-6335
Preprint. Discussion started: 6 November 2026
© Author(s) 2026. CC BY 4.0 License.

Lee, J. Y., Peterson, P. K., Vear, L. R., Cook, R. D., Sullivan, A. P., Smith, E., Hawkins, L. N., Olson, N. E., Hems, R., Snyder, P. K., and Pratt, K. A.: Wildfire smoke influence on cloud water chemical composition at Whiteface Mountain, New York, J. Geophys. Res.-Atmos., 127, e2022JD037177, https://doi.org/10.1029/2022JD037177, 2022.

Li, J., Wang, X., Chen, J., Zhu, C., Li, W., Li, C., Liu, L., Xu, C., Wen, L., Xue, L., Wang, W., Ding, A., and Herrmann, H.: Chemical composition and droplet size distribution of cloud at the summit of Mount Tai, China, Atmos. Chem. Phys., 17, 9885–9896, https://doi.org/10.5194/acp-17-9885-2017, 2017.

Li, J., Wu, H., Jiang, P., and Fu, C.: Rainwater chemistry in a subtropical high-altitude mountain site, South China: Seasonality, source apportionment and potential factors, Atmos. Environ., 268, 118786, https://doi.org/10.1016/j.atmosenv.2021.118786, 2022.

Lim, B., Jickells, T. D., and Davies, T. D.: Sequential sampling of particles, major ions and total trace metals in wet deposition, Atmos. Environ. A-Gen., 25, 745–762, https://doi.org/10.1016/0960-1686(91)90073-G, 1991.

Liu, L., Zhang, X., and Lu, X.: The composition, seasonal variation, and potential sources of the atmospheric wet sulfur (S) and nitrogen (N) deposition in the southwest of China, Environ. Sci. Pollut. Res., 23, 6363–6375, https://doi.org/10.1007/s11356-015-5844-1, 2016.

Liu, M., Song, Y., Xu, T., Xu, Z., Wang, T., Yin, L., Jia, X., and Tang, J.: Trends of precipitation acidification and determining factors in China during 2006–2015, J. Geophys. Res.-Atmos., 125, e2019JD031301, https://doi.org/10.1029/2019JD031301, 2020.

Liu, Y., Wang, W., Zhang, J., and Li, Z.: Characteristics and sources of chemical composition in precipitation on the Loess Plateau of China, Sci. Total Environ., 935, 173401, https://doi.org/10.1016/j.scitotenv.2024.173401, 2024.

Ma, L., Dadashazar, H., Hilario, M. R. A., Cambaliza, M. O., Lorenzo, G. R., Simpas, J. B., Nguyen, P., and Sorooshian, A.: Contrasting wet deposition composition between three diverse islands and coastal North American sites, Atmos. Environ., 244, 117919, https://doi.org/10.1016/j.atmosenv.2020.117919, 2021.

Monteiro, L. R., Terzer-Wassmuth, S., Matiatos, I., Douence, C., and Wassenaar, L. I.: Distinguishing in-cloud and below-cloud short and distal N-sources from high-temporal resolution seasonal nitrate and ammonium deposition in Vienna, Austria, Atmos. Environ., 266, 118740, https://doi.org/10.1016/j.atmosenv.2021.118740, 2021.

Paudel Adhikari, N., Adhikari, S., and Aryal, D.: Hydrochemical and isotopic characteristics on the southern and northern slopes of the Himalayas: Spatio-temporal controls and source apportionment, Sci. Total Environ., 949, 175147, https://doi.org/10.1016/j.scitotenv.2024.175147, 2024.

Ryu, Y.-H. and Min, S.-K.: Improving wet and dry deposition of aerosols in WRF-Chem: Updates to below-cloud scavenging and coarse-particle dry deposition, J. Adv. Model. Earth Sy., 14, e2021MS002792, https://doi.org/10.1029/2021MS002792, 2022.

Seinfeld, J. H. and Pandis, S. N.: Atmospheric Chemistry and Physics: From Air Pollution to Climate Change, 3rd edn., John Wiley & Sons, ISBN 978-1-118-94740-1, 2016.

https://doi.org/10.5194/egusphere-2026-6335
Preprint. Discussion started: 6 November 2026
© Author(s) 2026. CC BY 4.0 License.

Si, L. and Li, Z.: Atmospheric precipitation chemistry and environmental significance in major anthropogenic regions globally, Sci. Total Environ., 926, 171830, https://doi.org/10.1016/j.scitotenv.2024.171830, 2024.

Stein, A. F., Draxler, R. R., Rolph, G. D., Stunder, B. J. B., Cohen, M. D., and Ngan, F.: NOAA's HYSPLIT atmospheric transport and dispersion modeling system, B. Am. Meteorol. Soc., 96, 2059–2077, https://doi.org/10.1175/BAMS-D-14-00110.1, 2015.

Wang, Y., Xia, W., and Zhang, G. J.: What rainfall rates are most important to wet removal of different aerosol types?, Atmos. Chem. Phys., 21, 16797–16816, https://doi.org/10.5194/acp-21-16797-2021, 2021.

Wang, Z. F., Pan, X. L., Sun, Y. L., Xin, J. Y., Su, H., Cao, J. J., Li, J., Yang, T., Liu, H., Yao, W. J., Xu, W. Q., Chen, X. S., Zhou, W., Ma, Y. J., Cheng, X. L., Ye, J., Hu, B., Jiang, R. B., Wang, Z., Ge, B. Z., Wu, L., Li, X. W., Li, J. X., Wu, Z. C., Kong, L., Zhu, M. M., Jia, J., Li, X. Y., Fang, X. K., and Liu, L. Z.: Atmospheric Boundary Layer Eco-Environment Shanghuang Observatory: An integrated multiscale research platform in Southeastern China for understanding boundary layer processes, atmospheric chemistry feedback, and extreme weather–climate linkages, Adv. Atmos. Sci., 43, 1291–1299, https://doi.org/10.1007/s00376-025-5307-7, 2026.

Xie, Z., Xiao, H., and Xu, Y.: Organic acids in sequential volume-based rainwater samples in Shanghai: Seasonal variations and origins, Atmosphere, 13, 1502, https://doi.org/10.3390/atmos13091502, 2022.

Xu, D. H., Ge, B. Z., Wang, Z. F., Sun, Y. L., Chen, Y., Ji, D. S., Yang, T., Ma, Z. Q., Cheng, N. L., Hao, J. Q., and Yao, X. F.: Below-cloud wet scavenging of soluble inorganic ions by rain in Beijing during the summer of 2014, Environ. Pollut., 230, 963–973, https://doi.org/10.1016/j.envpol.2017.07.033, 2017.

Yang, F., Tan, J., Shi, Z. B., Cai, Y., He, K., Ma, Y., Duan, F., Okuda, T., Tanaka, S., and Chen, G.: Five-year record of atmospheric precipitation chemistry in urban Beijing, China, Atmos. Chem. Phys., 12, 2025–2035, https://doi.org/10.5194/acp-12-2025-2012, 2012.

Yao, L., Kong, S., Nemitz, E., Vieno, M., Cheng, Y., Zheng, H., Wang, Y., Chen, N., Hu, Y., Liu, D., Zhao, T., Bai, Y., and Qi, S.: Improving below-cloud scavenging coefficients of sulfate, nitrate, and ammonium in $PM_{2.5}$ and implications for numerical simulation and air pollution control, J. Geophys. Res.-Atmos., 129, e2023JD039487, https://doi.org/10.1029/2023JD039487, 2024.

Zeng, J. and Han, G.: Rainwater chemistry reveals air pollution in a karst forest: Temporal variations, source apportionment, and implications for the forest, Atmosphere, 11, 1315, https://doi.org/10.3390/atmos11121315, 2020.

Zeng, J., Han, G., Zhang, S., Xiao, X., Li, Y., Gao, X., Wang, D., and Qu, R.: Rainwater chemical evolution driven by extreme rainfall in megacity: Implication for the urban air pollution source identification, J. Clean. Prod., 372, 133732, https://doi.org/10.1016/j.jclepro.2022.133732, 2022.

Zhang, M., Wang, S., Wu, F., Yuan, X., and Zhang, Y.: Chemical compositions of wet precipitation and anthropogenic influences at a developing urban site in southeastern China, Atmos. Res., 84, 311–322, https://doi.org/10.1016/j.atmosres.2006.09.003, 2007.

https://doi.org/10.5194/egusphere-2026-6335
Preprint. Discussion started: 6 November 2026
© Author(s) 2026. CC BY 4.0 License.



Zhang, Y., Cao, Y., Tang, Y., Ying, Q., Hopke, P. K., Zeng, Y., Xu, X., Xia, Z., and Qiao, X.: Wet deposition of sulfur and nitrogen at Mt. Emei in the West China Rain Zone, southwestern China: Status, inter-annual changes, and sources, Sci. Total Environ., 713, 136676, https://doi.org/10.1016/j.scitotenv.2020.136676, 2020.

Zou, C., Yang, X., Zhang, Y., and Huang, H.: Characteristics and distribution of inorganic ions in segmented precipitation and contribution of below-cloud/in-cloud scavenging in Nanchang, Air Qual. Atmos. Health, 15, 903–916, https://doi.org/10.1007/s11869-022-01166-3, 2022.